NASA/TM—2012-217439

Wind Tunnel Testing of a One-Dimensional Laser Beam Scanning and Laser Sheet Approach to Shock Sensing

Roger Tokars, Grigory Adamovsky, Robert Anderson, Stefanie Hirt, and John Huang
Glenn Research Center, Cleveland, Ohio

Bertram Floyd
Sierra Lobo, Inc., Fremont, Ohio

March 2012

NASA STI Program . . . in Profile

Since its founding, NASA has been dedicated to the advancement of aeronautics and space science. The NASA Scientific and Technical Information (STI) program plays a key part in helping NASA maintain this important role.

The NASA STI Program operates under the auspices of the Agency Chief Information Officer. It collects, organizes, provides for archiving, and disseminates NASA's STI. The NASA STI program provides access to the NASA Aeronautics and Space Database and its public interface, the NASA Technical Reports Server, thus providing one of the largest collections of aeronautical and space science STI in the world. Results are published in both non-NASA channels and by NASA in the NASA STI Report Series, which includes the following report types:

- TECHNICAL PUBLICATION. Reports of completed research or a major significant phase of research that present the results of NASA programs and include extensive data or theoretical analysis. Includes compilations of significant scientific and technical data and information deemed to be of continuing reference value. NASA counterpart of peer-reviewed formal professional papers but has less stringent limitations on manuscript length and extent of graphic presentations.

- TECHNICAL MEMORANDUM. Scientific and technical findings that are preliminary or of specialized interest, e.g., quick release reports, working papers, and bibliographies that contain minimal annotation. Does not contain extensive analysis.

- CONTRACTOR REPORT. Scientific and technical findings by NASA-sponsored contractors and grantees.

- CONFERENCE PUBLICATION. Collected papers from scientific and technical conferences, symposia, seminars, or other meetings sponsored or cosponsored by NASA.

- SPECIAL PUBLICATION. Scientific, technical, or historical information from NASA programs, projects, and missions, often concerned with subjects having substantial public interest.

- TECHNICAL TRANSLATION. English-language translations of foreign scientific and technical material pertinent to NASA's mission.

Specialized services also include creating custom thesauri, building customized databases, organizing and publishing research results.

For more information about the NASA STI program, see the following:

- Access the NASA STI program home page at *http://www.sti.nasa.gov*

- E-mail your question via the Internet to *help@sti.nasa.gov*

- Fax your question to the NASA STI Help Desk at 443–757–5803

- Telephone the NASA STI Help Desk at 443–757–5802

- Write to:
  NASA Center for AeroSpace Information (CASI)
  7115 Standard Drive
  Hanover, MD 21076–1320

NASA/TM—2012-217439

Wind Tunnel Testing of a One-Dimensional Laser Beam Scanning and Laser Sheet Approach to Shock Sensing

Roger Tokars, Grigory Adamovsky, Robert Anderson, Stefanie Hirt, and John Huang
Glenn Research Center, Cleveland, Ohio

Bertram Floyd
Sierra Lobo, Inc., Fremont, Ohio

National Aeronautics and
Space Administration

Glenn Research Center
Cleveland, Ohio 44135

March 2012

Acknowledgments

The work was supported by the Hypersonic Project under the NASA's Fundamental Aeronautics Program. The authors would like to acknowledge Dave Saunders, Scott Smrdel, Randall Chriss and the rest of those in the W-6b wind tunnel facility for their help and valuable advice on flow mechanics and control. Moreover, one of the co-authors, John Huang, appreciates the support from the NASA Undergraduate Student Research Program and the NASA Glenn Universities Affairs Office. The authors also appreciate the help of James Williams for setting up the experimental optical systems.

This work was sponsored by the Fundamental Aeronautics Program
at the NASA Glenn Research Center.

Level of Review: This material has been technically reviewed by technical management.

Available from

NASA Center for Aerospace Information
7115 Standard Drive
Hanover, MD 21076–1320

National Technical Information Service
5301 Shawnee Road
Alexandria, VA 22312

Available electronically at http://www.sti.nasa.gov

Wind Tunnel Testing of a One-Dimensional Laser Beam Scanning and Laser Sheet Approach to Shock Sensing

Roger Tokars, Grigory Adamovsky, Robert Anderson, Stefanie Hirt, and John Huang*
National Aeronautics and Space Administration
Glenn Research Center
Cleveland, Ohio 44135

Bertram Floyd
Sierra Lobo, Inc.
Fremont, Ohio 43420

Abstract

A 15- by 15-cm supersonic wind tunnel application of a one-dimensional laser beam scanning approach to shock sensing is presented. The measurement system design allowed easy switching between a focused beam and a laser sheet mode for comparison purposes. The scanning results were compared to images from the tunnel Schlieren imaging system. The tests revealed detectable changes in the laser beam in the presence of shocks. The results lend support to the use of the one-dimensional scanning beam approach for detecting and locating shocks in a flow, but some issues must be addressed in regards to noise and other limitations of the system.

Introduction

Airborne vehicles moving through the atmosphere with a speed above that of sound may generate shock waves. The shock waves may be either detached from the flying vehicle like, for instance, bow shocks or attached to the vehicle's internal or external surfaces like normal or oblique shocks. Formation and propagation of aerodynamic shocks are important considerations in the design of in-flight control systems and in the performance evaluation of individual components in ground test facilities (Refs. 1 to 3). Moreover, monitoring of aerodynamic shocks and their interactions enhances the safety and performance of supersonic and hypersonic flights (Refs. 4 and 5).

The need to develop shock position sensors capable of meeting flight qualifying requirements was especially emphasized during the High Speed Commercial Transport (HSCT) development (Refs. 6 and 7). In the process, various approaches were analyzed and sensor prototypes were developed and tested (Refs. 8 and 9). Early efforts were concentrated around using pressure taps along the inlet walls. The positions of the shocks were determined by tracking the pressure reading and locating the pressure jump associated with the shock. This basic technique evolved in several wall pressure-based configurations of normal shock position sensing systems. Despite an apparent initial success, these wall pressure-based measuring techniques had serious drawbacks. The most important drawbacks were slow response due to pneumatic manifolds used and the effect of the boundary layer on the stability of pressure readings. These problems seriously restricted applicability of these techniques to normal shock detection and control during supersonic flight. Moreover, for a commercial aircraft, economic efficiency has to be achieved in order to make supersonic flight economically viable. As a result, the flight control system is required, in addition to avoiding a un-start, to provide the most economical operating regime for the engine (achieved by minimizing the fuel consumption).

Optical flow visualization has been widely used in ground-based flow analyzing facilities. Instrumentation and measurement schemes used in these cases have typically included well-known flow visualization techniques such as shadowgraph, Schlieren, and interferometry (Refs. 10 to 13). Advantages

*NASA Undergraduate Student Research Program

of these techniques include the ability to view large areas which allows examination of shock structure. However, these techniques do not lend themselves to in-flight or ground-based shock sensing inside flow passages requiring, as they do, optical access, and large optical components. An alternative technique involving a scanning laser beam is presented here which has the potential for on-board real-time determination of shock location. The technique is based on changes in a laser beam profile as the beam interacts with a shock (Refs. 14 to 16).

The scanning beam technique was previously tested using an optical fiber, with known optical properties and fixed location, to simulate the effects of a shock (Ref. 17). In this paper, we have continued development of the technique by deploying the beam scanning equipment in a supersonic wind tunnel. A one-dimensional laser sheet measurement technique using the same hardware was also tested in the wind tunnel.

Beam Propagation through Shocks

The theory of the propagation of electromagnetic radiation through media interfaces can be found in numerous references (Refs. 18 to 22). Scattering patterns that result have been studied analytically and experimentally. Characteristic scattering patterns and the underlying physics have been demonstrated and explained (Refs. 23 to 29).

In the case of high speed aerodynamic flows, shock waves that may occur create abrupt density gradients and thus abrupt changes in index of refraction (Refs. 30 and 31). Experiments performed with a bluff body inserted in a supersonic flow have demonstrated laser beam scattering from the bow shocks formed in the process of the flow interaction with the bluff body (Ref. 14).

It is clear from the work presented in References 14 and 17 that the light scattering observed in a stationary focused laser beam may allow for locating of aerodynamic shocks. Extending this idea beyond a point location, the use of a laser sheet to detect changes across a whole range of locations has been demonstrated in laser sheet shadowgraph configurations (Ref. 32). This paper further investigates the stationary focused laser beam and laser sheet methods with the addition of the scanning focused beam method in a supersonic flow with shocks.

Scanning Beam Technique

Principle of Operation

The shock detection technique reported here is based on scattering of a laser beam passing through aerodynamic shocks. As was mentioned above, experimental results as well as computational analyses have described the changes in the beam profile that result from those interactions (Refs. 14 and 26). In past work, the changes manifested as beam spreading, formation of tails and secondary fringes perpendicular to the shock. In a supersonic flow such changes in the beam profile may be used to obtain a greater understanding of the shock such as its strength and thickness. In this work, we attempted to locate the shock based on scattering of a laser beam. Using the changes in the laser beam profile, shock detection techniques using a small diameter laser beam have been devised. In the beam scanning technique presented in this paper, referred to hereafter as the Beam Scanning Mode, a laser beam is reflected from a mirror mounted on an electromagnetic rotary actuator with a 20° excursion range. In addition to the Beam Scanning Mode, a Laser Sheet Mode is also created by simply stopping the mirror and reflecting the laser beam through an optical fiber which acts like a cylindrical lens and spreads the beam into a sheet. In both modes, the beam image is recorded on a CCD line camera detector and changes in the beam image are analyzed to determine the shock locations. The Laser Sheet Mode utilizes essentially the same hardware as the Beam Scanning Mode, thus the two modes can be transitioned, or reconfigured back and forth quickly. This system is henceforth called the **Reconfigurable Beam and Sheet** system, or **RBS** system for short. With the capability to switch between both modes, the experimenter can utilize whichever mode is most advantageous.

Experimental Setup

The experimental setup of the Beam Scanning Mode used for this work is shown in Figure 1. A Helium-Neon laser beam is reflected from a rotating mirror, sent through a telescope and imaged onto a CCD line camera. The flowpath of interest lies between the two lens elements of the telescope as shown in Figure 1. Neutral density filters are inserted, as needed, into the beam path to eliminate sensor saturation. All major components are mounted on a rail that permits change of the relative distance between them. The laser emits a 0.48 mm diameter beam at 0.6328 μm wavelength. This diameter beam was chosen because it was readily available in the lab. The data indicates the beam image subtends approximately 65 pixels in diameter which is equal to approximately 0.57 cm based on the 4.5 cm scan range and the 512 camera array size. This provided for a beam narrow enough for effective scanning.

During alignment, adjustments are made to the optical equipment locations and scanning parameters so that the entire beam and scan range are captured with the CCD line camera. The Beam Scanning Mode seen in Figure 2(a) shows the angle θ that the laser beam makes from the center position, $\theta = 0°$. The angle θ is determined by a voltage input to the mirror controller. The waveform of the voltage input determines the scan pattern, such as a sine wave, sawtooth wave, or triangle wave. During testing the triangle wave is used so that the scan pattern positions the laser at each location for an equal amount of time for consistent pixel intensity illumination. The optical fiber seen as a dot near the mirror in Figure 2(a) is not utilized as it is outside the scanning range in Beam Scanning Mode.

In the experimental setup for the Laser Sheet Mode, the mirror is set to the angle φ where the laser is directed through an optical fiber as seen in Figure 2(b). The optical fiber scatters the beam into a sheet. The distance between the optical fiber and the collimating lens is approximately the focal length of the collimating lens, which collimates the laser sheet through the flowpath. The angle φ is greater than θ so that the Laser Sheet Mode doesn't interfere with the Beam Scanning Mode. Before testing, slight adjustments in the location of the optical fiber were done with a remote actuator to improve the uniformity of the imaged laser sheet.

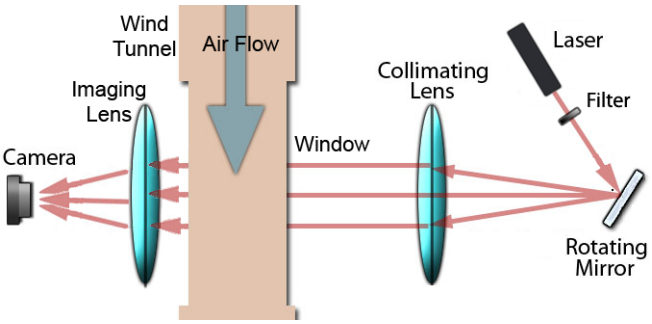

Figure 1.—Experimental setup for the scanning approach. Distances are not to scale.

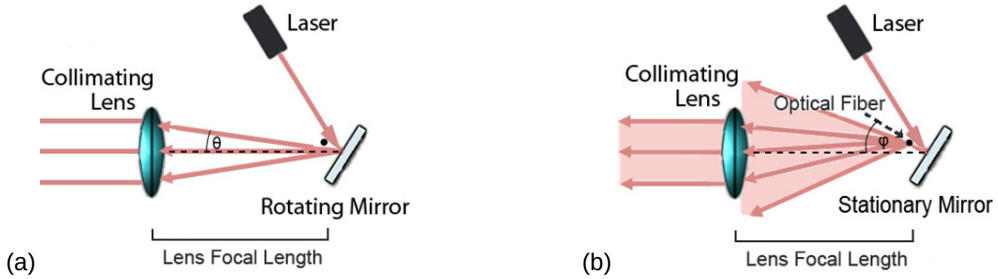

Figure 2.—RBS system split up into: (a) Schematic of the Beam Scanning Mode with rotating mirror scanning a focused laser beam across a path from angles –θ to +θ in the horizontal plane. (b) Schematic of the Laser Sheet Mode where a light sheet is created using a stationary mirror at angle φ to reflect the beam through an optical fiber.

A photograph of the RBS setup is shown in Figure 3 with dimensions given in Figure 4. The collimating and imaging lenses have a focal length of 15 and 35.5 cm, respectively. Both lenses have a diameter of approximately 7 cm. The camera is positioned at a distance inside the focal length of the imaging lens so the complete scan range is imaged across the CCD array. This setup was used in all experiments discussed in this paper.

The RBS system uses a computer to generate a voltage which controls the rotating mirror to direct the laser beam at a desired location in the flow. A calibration of the mirror system was done before each test run. This involved using a triangle wave to scan the beam across the camera pixel array and processing the image to correlate laser center position to mirror voltage. A typical calibration of the setup in the wind tunnel is shown in the Position versus Voltage plot in Figure 5 utilizing a triangle wave. In this figure the curvature of the plot is due to the effect of the lens used to collimate the laser beam. A fifth order polynomial equation is fit to the data to correct for this curvature. The position of the laser is then known for any mirror voltage. In order to keep the beam scanning range within the linear portion of the position versus voltage function, the voltage range was kept within ±1 V. The resulting scan range was 4.5 cm in width.

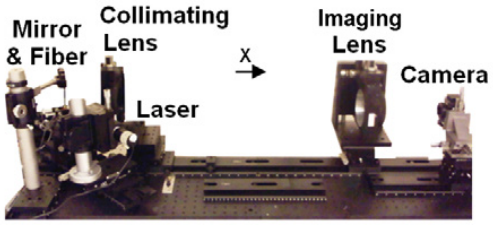

Figure 3.—RBS setup as seen from the side viewpoint to scale.

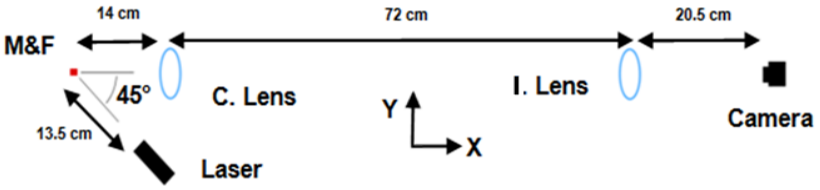

Figure 4.—RBS setup as seen from the top viewpoint to scale.

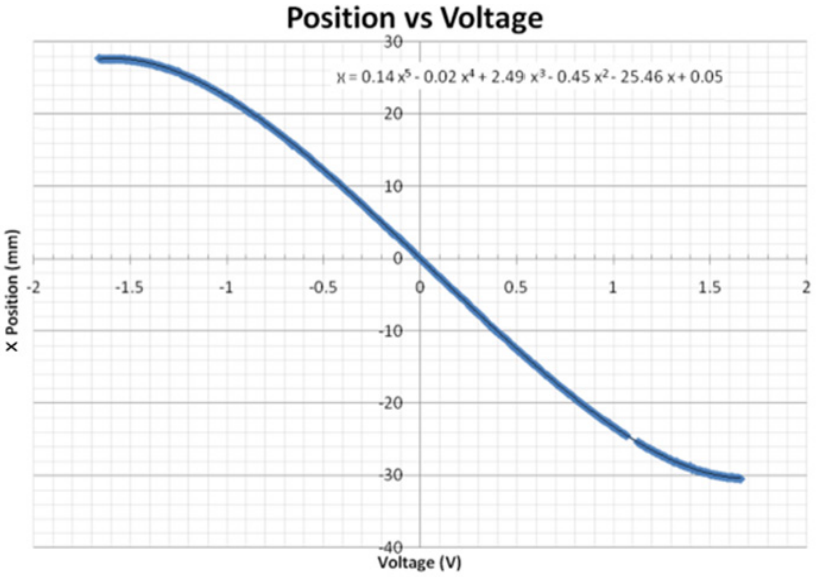

Figure 5.—Calibration of the rotating mirror voltage to laser beam position.

The scanning system was tested in the NASA Glenn Research Center 15- by 15-cm supersonic wind tunnel, seen in Figure 6. During the testing, the flow was measured at Mach 2, with a total pressure of approximately 19.33 psia. The wind flow total temperature was 536.16 °R. The dew point was approximately –19 °C. The Reynolds number was varied between 4×10^6/ft to 8×10^6/ft.

The RBS system scan range is seen through the wind tunnel window in Figure 7. The scan range, approximately 4.5 cm, can be seen as a red line on the front window. Reflections can also be seen in the rear window.

Control of the shock position was done using a movable ramp inside the wind tunnel, hereafter called the Oblique Shock Generator, diagrammed in Figure 8. The ramp was located in the upper section of the wind tunnel, above the window seen in Figure 7. The ramp was a flat piece of metal that extended across the tunnel from wall to wall. The ramp was tilted at specified angles, δ, to move the oblique shocks, denoted with dashed lines. As expected, the incident and reflected shocks were the strongest shocks observed. These shocks were the focus of the measurements with the RBS system and the Schlieren system.

The Oblique Shock Generator ramp angles were varied between 0° and 10°. The standard deviation of the angle setting was 0.03°. Typical shock structures for the various angles are shown in Figure 9. The ramp angle was set to 0° for the Prestart Condition. After the Prestart Condition was achieved, the ramp was then slowly rotated to 9°, which brought the incident and reflected shocks into the viewable area and within the RBS scan range. Ramp angles from 9° to 9.8° were called the Test Inspection Condition because several measurements were taken in this angle range to investigate the response of the RBS system. As the ramp angle was increased to 10° and greater, the shocks became less stable and more likely to go into the Unstart Condition. At the Unstart Condition the flow below the ramp is sub-sonic, the oblique shocks in the scan range disappear and a normal shock sits upstream.

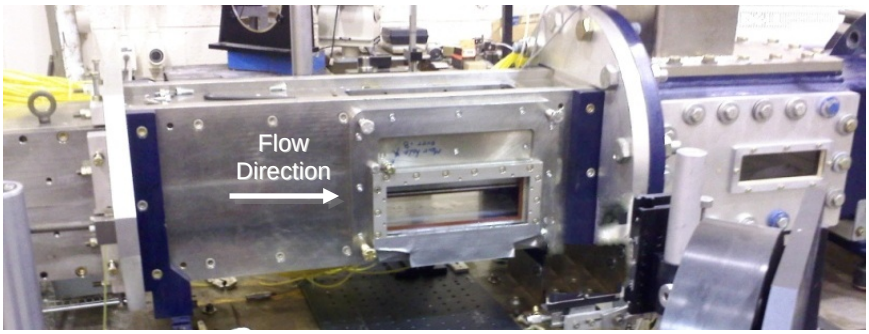

Figure 6.—The 15- by 15-cm supersonic wind tunnel with Schlieren mirrors in the fore and background.

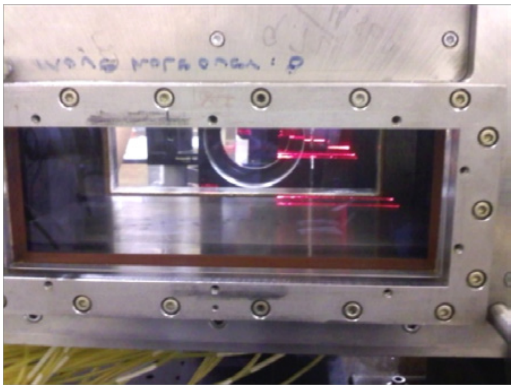

Figure 7.—RBS system's scan range as seen through the wind tunnel window.

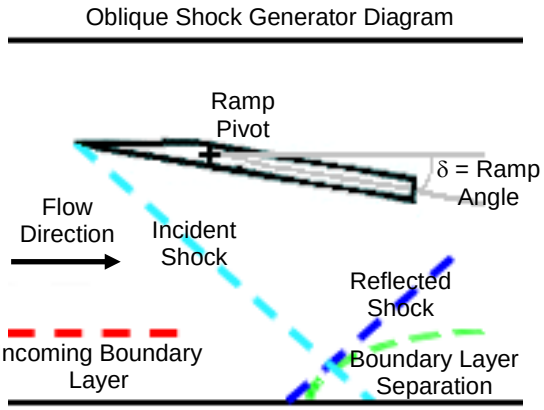

Figure 8.—Diagram of the Oblique Shock Generator that controls the oblique shocks in the wind tunnel.

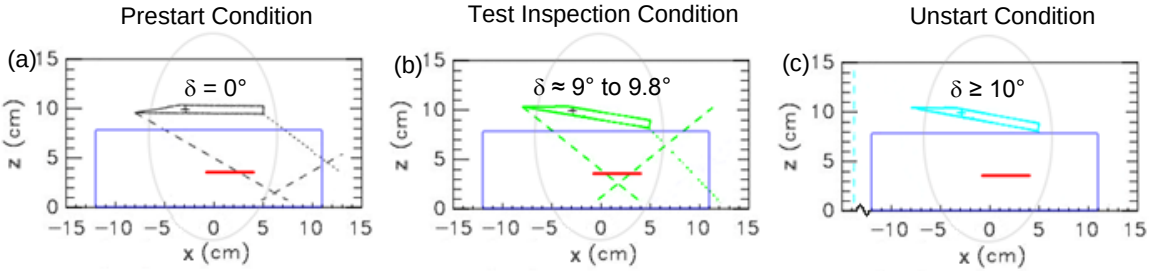

Figure 9.—Expected shock structure for various ramp angles inside the 15- by 15-cm wind tunnel. The blue rectangle is the viewable area through the wind tunnel window. The RBS system's scan range is shown by the red line. The Schlieren viewing area is denoted by a grey ellipse. Shocks of interest are colored dashed lines. As the ramp angle is increased the shocks move upstream relative to the scan range. (a) 0° ramp angle, Prestart Condition. (b) 9° to 9.8° ramp angle, Test Inspection Condition, and (c) 10° and greater ramp angle, Unstart Condition.

For a comparison with the RBS system results, the shock structure was also imaged with the tunnel Schlieren system to visualize shock stability and position. The Schlieren system elements in this wind tunnel include an arc lamp with its light directed through a pin hole, two 8-in. diameter spherical mirrors, two 10-in. diameter turning mirrors, and a knife edge. The Schlieren viewing area is approximately 55 percent of the wind tunnel window as outlined by the grey ellipse seen in Figure 9. Schlieren images were captured and recorded at 30 frames per second. The shock structure was somewhat unstable; but it generally oscillated about a location that was repeatable given the same test conditions such as temperature, flow velocity, and ramp angle. From the Schlieren images, we estimate that the reflected shock thickness was less than 1 cm and exhibited a center oscillation range of less than 0.5 cm for any set ramp angle. The repeatability of the ramp angle (estimated at 0.03°) translated into a negligible shock movement. We could not take both Schlieren and RBS data at the same time because the RBS system obstructed the optical path of the Schlieren system, so the tunnel flow was turned off and the Schlieren system was replaced with the RBS system scanning line overlapping the shock position observed in the Schlieren images. The wind tunnel was brought up to the same flow conditions and ramp angle to create approximately the same shock position. Thus, a comparison between the Schlieren system and the RBS system could be done.

Image Processing

Software was developed to detect and locate shocks using the images from the RBS system. Software was developed for the two data acquisition modes used in this work: the Beam Scanning Mode and the Laser Sheet Mode. A third technique based on two-dimensional imaging of the beam profile of a scanning laser was studied in previous work (Ref. 14), but the data acquisition rate for this technique was deemed too slow to adequately image the rapidly changing shock structure in the wind tunnel.

Beam Scanning Mode

In the Beam Scanning Mode, the RBS system uses a 65k frames per second line camera (Ref. 35) to image the laser beam as the beam is scanned, as seen in Figure 2(a). Although the beam scattering effects are two-dimensional, only a one-dimensional line camera is used in this work because of its much higher frame rate.

A more detailed description of the Beam Scanning Mode follows. One single row of image data is collected and time tagged by the line camera at a time. The beam appears as a bright spot in each camera image. Each row of data is temporarily stored in an array. The process of saving data and scanning the laser repeats until a designated number of lines are acquired. The result is an image array in which each row of data contains the line camera pixel intensities at a time denoted by its position in the image column. The time between lines is determined by the camera scan rate. Because the images are saved as the laser beam is scanned, a diagonal line is present in the resulting image representing the locus of the laser spot position at each time increment. Figure 10 shows three images from the Beam Scanning Mode taken before the wind tunnel was brought up to speed in order to verify the system was properly setup. The image width is equal to the scan width (4.5 cm) and time increases from top to bottom. The scan frequency was 63 Hz, which equates to 16 ms duration from top to bottom. Figure 10(a) is a reference image, which is a typical beam scan without any beam scattering within the scan range. Figure 10(b) is a beam scan with a 2.4 mm diameter opaque capillary tube placed within the scan range. The opaque tube caused a shadow or decrease in the laser spot brightness to appear in the image. Figure 10(c) is a beam scan with a small air jet within the scan range. The air jet came out of the capillary tube with an inner diameter of approximately 1.4 mm. The jet resulted in a fluctuation of the density in the path of the laser scan, thus the imaged laser intensity fluctuated at this location. Placing an opaque tube within the scan range at a known position is a useful calibration technique for determining the limits and consistency of the scan. Likewise, placing the air jet within the beam scan caused the light to scatter from its normal path providing for a simple demonstration of the sensitivity of the setup.

Additional imaging analysis is done by comparing the reference image to images with the effects of the flow (for example comparing Figure 10(a) to Figure 10(b) and (c)). The images are subtracted from each other to mitigate the systematic effects of defects seen in the lenses, windows, and mirrors. The standard deviation of the images was also computed to analyze variations in the flow. These additional imaging analysis techniques are discussed later in this paper.

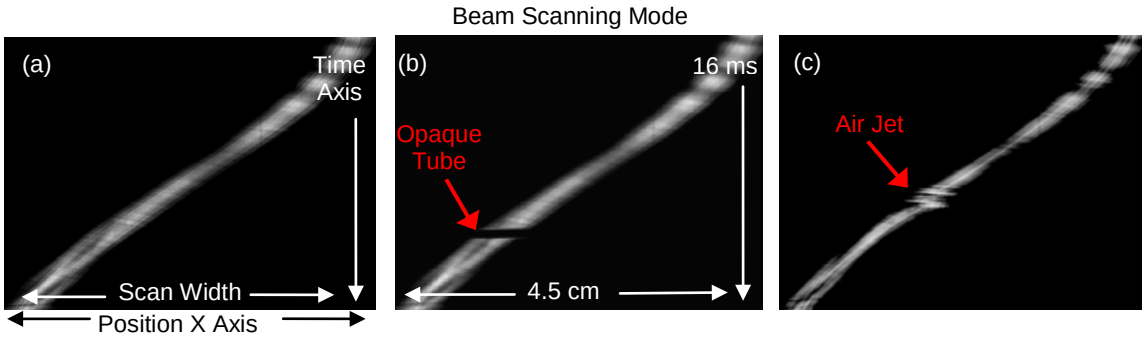

Figure 10.—Demonstration of the Beam Scanning Mode (a) reference, (b) with an opaque tube, and (c) with an air jet placed within the scanning range.

Laser Sheet Mode

The RBS system also uses the same 65k frames per second line camera in the Laser Sheet Mode to take one-dimensional images of the profile of a laser sheet, propagated across a given range, as seen in Figure 2(b). This mode improves upon the Beam Scanning Mode by not requiring the use of a scanning beam. As a result, the Laser Sheet Mode was up to 50 times faster than the Beam Scanning Mode for gathering data across the entire inspection area with the equipment used in this report.

A more detailed description of the Laser Sheet Mode follows. Similar to the Beam Scanning Mode, one single row of data is collected by the line camera at a time. A row of data is temporarily stored in an array. As time passes, this process repeats to generate an image containing the designated number of lines. Unlike the Beam Scanning Mode, the camera captures the image of the cross-section of a stationary laser sheet spanning the entire line camera width. Figure 11 shows three images from the Laser Sheet Mode taken before the wind tunnel was brought up to speed in order to verify the system was properly setup. The image width is equal to the sheet width (4.5 cm) and the time increases from top to bottom. The camera was capturing at about 65k frames per second. There are 508 rows in the images below. This equates to 8 ms duration from top to bottom for each image. Figure 11(a) is a reference image, which is a typical scan without any beam scattering within the sheet width. Figure 11(b) is a scan with a 2.4 mm diameter opaque capillary tube, just as in Figure 10(b), placed within the sheet width. Figure 11(c) is a laser sheet scan with a small air jet within the sheet width. Just as in Figure 10(c), the air jet came out of the capillary tube with an inner diameter of approximately 1.4 mm. The air jet created a fluctuation of the density in the path of the laser sheet, thus the laser intensity fluctuates. Placing an opaque tube within the sheet width at a known position is a useful calibration technique for determining the limits and consistency of the scan range. Likewise, placing the air jet within the sheet width caused the light to scatter from its normal path providing for a simple demonstration of the sensitivity of the setup.

Other vertical lines present in Figure 11 are caused by the optical fiber used to form the laser sheet, as well as by scattering and reflections from the wind tunnel windows and lenses. Such noise was low enough to ignore and/or mitigate by corrective measures such as additional image processing and analysis.

Data

To test the Reconfigurable Beam and Sheet (RBS) system in the NASA Glenn 15- by 15-cm supersonic wind tunnel, the wind tunnel was operated using three measurement techniques including:

A. Schlieren imaging—To provide a reference with which to compare our results.
B. RBS in Beam Scanning Mode.
C. RBS in Laser Sheet Mode.

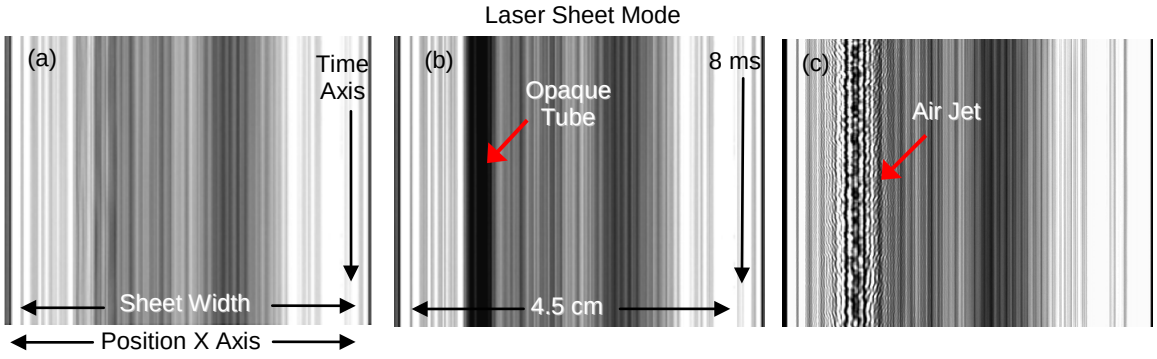

Figure 11.—Image from the Laser Sheet Mode (a) reference, (b) with an opaque tube, and (c) with an air jet placed within the sheet range.

Measurements were made at three Reynolds numbers. At each Reynolds number setting, measurements were made at several ramp angles. Finally, measurements were made during the transition to unstart. The wind tunnel Reynolds numbers and ramp angles for these tests are shown in Table I. The exact angle at which unstart occurred varied slightly due to the unsteady nature of the shock. Thus, that angle is not shown in the table. Unstart typically occurred at a ramp angle greater than 9.80°.

TABLE I.—TEST MATRIX OF WIND TUNNEL REYNOLDS NUMBERS AND RAMP ANGLES.

Reynolds Number	Ramp Angle δ
7.5×10^6/ft	9.50°
7.5×10^6/ft	9.65°
7.5×10^6/ft	9.80°
5.04×10^6/ft	9.00°
5.04×10^6/ft	9.24°
5.04×10^6/ft	9.48°
4.11×10^6/ft	9.00°
4.11×10^6/ft	9.24°

The shock location is dependent on both the Reynolds number and ramp angle. Increasing the Reynolds number and increasing the ramp angle shifted the shock downstream and upstream respectively. For the three Reynolds numbers the results and analysis were similar for ramp angle induced shock movements. In the interest of brevity all results and discussion hereafter are for testing with a Reynolds number of 7.5×10^6/ft.

Schlieren Measurements

Schlieren images with various ramp angles are shown in the first column of Figure 12, Figure 13(a), and (b). The flow is brought to the initial Prestart Condition with a 0° ramp angle. The shock structure for this condition is shown in the Schlieren image of Figure 13(a) and diagrammed in Figure 9(a). The incident shock is clearly visible. Increasing the ramp angle to approximately 9° shifts the reflected shock and the boundary layer separation upstream and eventually brings them into view in the Schlieren image, as diagrammed in Figure 9(b) as the Test Inspection Condition. Schlieren image of ramp angle 9.50° is shown in Figure 12(a) with the reflected shock position represented by the blue colored line. The green and red colored lines represent the superimposed reflected shock location for ramp angles 9.65° and 9.80°, respectively. Schlieren images of ramp angles 9.65° and 9.80° are shown in Figure 12(b) and (c), respectively, with corresponding superimposed lines for the ramp angles as well. These same ramp angles were used in testing with the Beam Scanning and Laser Sheet Modes seen in the second, third, and fourth column of Figure 12. Increasing the ramp angle beyond approximately 9.8° resulted in the Unstart Condition seen in Figure 13(b) and diagrammed in Figure 9(c). All of the images have the flow direction going from left to right.

Beam Scanning Tests

Results from the Beam Scanning tests are shown in the second and third columns of Figure 12 and in Figure 13(d). The approximate scan location in the wind tunnel is shown in Figure 9. For each flow condition, approximately three minutes of data were collected at each scan frequency of 16, 32, 64, 126, 254, 508, 1016, and 1270 Hz. The different scan frequencies were tested to explore the operating envelope of the system. For example, the faster scan frequency corresponds to an increase in the update rate of the tracked position of the shock. A drawback of an increased scan frequency is that the shock is illuminated for a shorter period of time, making it more difficult to locate. A Beam Scanning Mode single scan cycle is shown in the second and third column of the images of Figure 12. One scan cycle is the scan

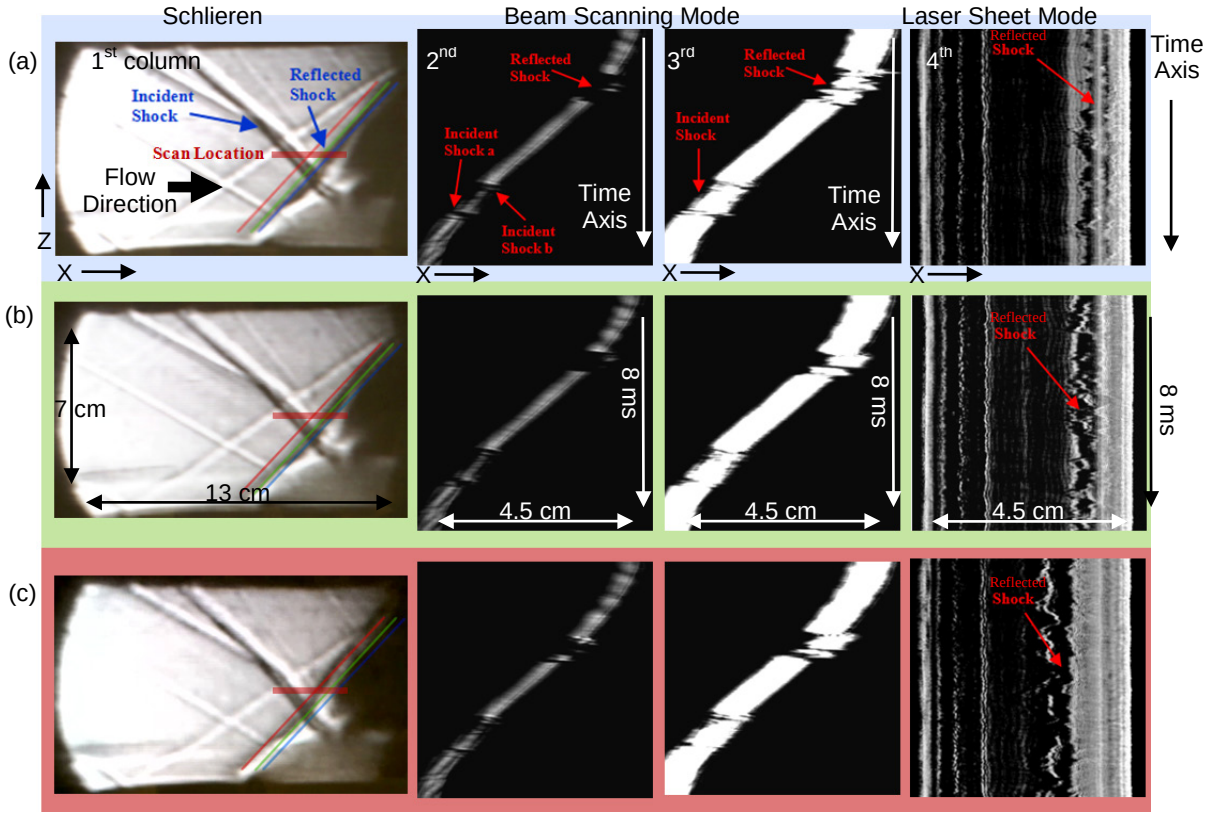

Figure 12.—Static test condition with ramp angles: ((a) blue) 9.50°, ((b) green) 9.65°, and ((c) red) 9.80°. Schlieren images are shown in the first column, Beam Scanning Mode for the over and underexposed settings in the second and third column respectively, and Laser Sheet Mode in the fourth column.

of the laser from left to right, or right to left across the entire scan range (4.5 cm). The second column of Figure 12 is the underexposed scan, while the third column in this figure is the overexposed scan. The overexposed scan used an unfiltered laser beam. The underexposure scan used neutral density filters to reduce the laser intensity. The frequency of the scan in both columns of images is 126 Hz which equates to 8 ms for each scan. The Beam Scanning Mode images have ramp angles 9.50°, 9.65°, and 9.80° for Figure 12(a), (b), and (c), respectively. The underexposure scan demonstrates the sensitivity of the Beam Scanning Mode. The overexposed scan demonstrates that the effect of the shocks can still be visualized while allowing for transition from Beam Scanning Mode to Laser Sheet Mode with the same initial laser beam intensity. The underexposed scan utilized a beam intensity too low for Laser Sheet Mode. The Laser Sheet Mode requires a stronger initial laser beam because the laser light is spread over a larger area. As a comparison to the measurements of a static shock, the measurements of a fast moving shock during the jump to unstart are shown in Figure 13(d). Eight scan cycles are shown in each image because more than one cycle was necessary to capture the movement of the shock transition to unstart. Figure 13(d) images are ordered from left to right corresponding to scan frequencies of 126, 508, 1016, and 1270 Hz respectively. All of the images have the flow direction going from left to right.

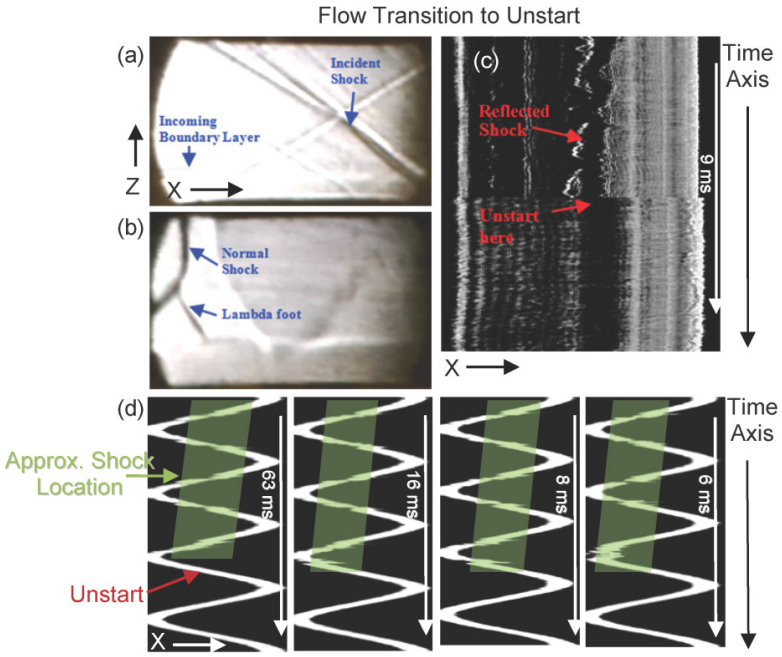

Figure 13.—Dynamic test condition results. Schlieren image showing (a) prestart, 0° ramp angle, (b) unstart, 10° ramp angle. (c) Laser Sheet Mode showing transition to unstart. (d) Scanning Beam Mode showing transition to unstart for scanning frequencies 126, 508, 1016, and 1270 Hz with shock location shown in green.

Laser Sheet Tests

Results from measurements in the Laser Sheet Mode are shown in the fourth column of Figure 12. The approximate scan location in the wind tunnel is shown in Figure 9. For each flow condition, approximately three minutes of data were collected. Only a portion (8 ms) of data that was collected is shown for each image. One row of data in Laser Sheet Mode contrasts to the several rows required to capture one transition of the laser scan across the image in Beam Scanning Mode. Both Laser Sheet Mode and Beam Scanning Mode tests used the same scan range (4.5 cm). Figure 12 images have ramp angles 9.50°, 9.65°, and 9.80° for (a), (b), and (c), respectively. Figure 13(c) shows Laser Sheet Mode data within which the transition to Unstart Condition occur. The shock location is apparent from the area of the image where the greatest deviation occurs as we move from top to bottom. Notice the similarity between this shock image pattern and the pattern observed in the air jet test shown in Figure 11. The vertical lines associated with the Laser Sheet Mode are the noise from the system and ways of mitigating these effects are discussed later in the report. All of the images have the flow direction going from left to right.

Comparing the Schlieren images to results from the Beam Scanning and Laser Sheet Modes, both techniques show a significant movement of the reflected shock upstream when the ramp angle is increased, while the incident shock movement is very small. Operational constraints prevented use of the Schlieren system simultaneously with the line scan camera. Thus, the approximate location of the scan line in the Schlieren image was determined by marking where the laser scan passed through the wind tunnel window. This marked location was then visualized on the Schlieren image. The reflected shock in the Schlieren image, seen in Figure 12, is believed to correspond to the downstream detected shock in the Beam Scanning and Laser Sheet results. The reflected shock appears to be more pronounced with greater spatial variation, suggesting it is a stronger shock than the incident shock. Such a strong reflected shock is expected right before the boundary layer separation. Much of the fine detail is lost in the overexposed

images because of saturated pixels, especially at the location of the shocks. The incident shock location is more easily seen in the underexposed images. In the underexposed images, details are seen at the incident shock location which is split up into ‘a’ and an even smaller ‘b’ component. The split incident shock is seen in the Schlieren images of Figure 12 where the scan location intersects the incident shock. These shocks are actually made up of the incident shock and most likely a Mach wave coming off a defect or edge of the top wall. The Laser Sheet Mode tracked the reflected shock, but the somewhat weaker incident shock was only visible under closer inspection. Results suggest that the laser sheet light distribution should be more even to provide for a brighter image over the whole sheet. This is of particular concern when the reflected shock travels upstream in the darker areas as seen in Figure 12 in the Laser Sheet Mode for 9.80° ramp angle. This dark area became an issue only when the flow was turned on, as the reference image in Figure 11(a) showed a much brighter and uniform laser sheet.

One limitation in the Beam Scanning Mode resulted from the motorized scanning mirror having a maximum oscillating frequency of approximately 635 Hz. For a beam traveling back and forth in one period, the maximum scan rate across the shocks for the Beam Scanning Mode would be twice the 635 Hz mirror frequency, or approximately 1270 Hz scan rate. During testing, the beam scan rate ranged from 16 to 1270 Hz. Although the lower speed scans had more lines of data per scan to inspect the shock with, the high speed of the shock movement made it difficult to track the exact instantaneous location of the shock, thus the shock appeared to jump around.

The transition to unstart occurred extremely fast and also unpredictably. As the exact ramp angle where unstart occurred was unknown and inconsistent, the ramp angle was simply increased until unstart occurred. To acquire data during the steady to unstart transition, the flow was prestarted with the ramp angle set at 0°, as seen in Figure 13(a). The angle was then slowly increased until a stable shock appeared in our area of inspection. Data collection was then begun and the ramp angle was then increased until an unstart transition occurred. Figure 13(c) suggests that even the 65 kHz Laser Sheet Mode could not easily follow the rapid transition to unstart, although a lower signal to noise ratio is also a contributing factor. The Beam Scanning Mode, even though it was a slower scan speed than the continuous Laser Sheet Mode, could track the shock reasonably well when scanning direction was in the same direction as the shock movement. This means that the right to left scanning of the laser had the chance to follow the shock as it transitioned from steady (right) to unstart (left and beyond) state, as seen in Figure 13(d). Observing the flow after unstart occurs, such as in Figure 13(c), it is apparent that the new flow conditions shift and change the visualized laser sheet. Such a change in the laser sheet must be taken into account during image analysis of the flow. The distortion of the laser sheet in the unstart condition was also different from laser sheet in the flow off condition.

Data Processing and Analysis

Custom software allowed for data processing and analysis of the test results which provided for an automated and consistent way to determine the shock locations. The shock locations are identified by determining where the laser beam deviates from its usual path. Three data processing methods are used in this report. They are referred to as Reference Standard Deviation Processing, Flow Standard Deviation Processing, and Laser Sheet Subtraction Processing. These three data processing methods all utilize the “X” subarray analysis described later in this section.

The Reference Standard Deviation Processing, used exclusively in Beam Scanning Mode, involves comparing the images saved in testing with a shock present, to the reference image with no shock present. Images with the shock present are compared to the reference image by taking the standard deviation at each pixel location.

$$s = \sqrt{\frac{1}{N-1}\sum_{i=1}^{N}\left(x_i - \bar{x}\right)^2} \tag{1}$$

$N = 2$ is the number of images compared.
x is the pixel intensity.
$\bar{x}$ is the average pixel intensity at that particular location across all images.
i is the image index.

The Flow Standard Deviation Processing, also exclusively used in Beam Scanning Mode, extends the standard deviation calculation in Equation (1) taking the standard deviation across N = 500 images with the shocks present instead of just the reference image. The pixel values in these results indicate variability in pixel values across many images. The assumption is that high variability indicates the presence of a shock boundary.

The comparison between the Reference Standard Deviation Processing and Flow Standard Deviation Processing methods was done to determine whether the faster Reference Standard Deviation Processing method is comparable to the much slower Flow Standard Deviation Processing method. Although faster, the Reference Standard Deviation Processing method is not always possible. This is because a reference image is defined as an image without the presence of a shock in the flow, yet removing the shock can change the flow dynamics resulting in a reference image that doesn't relate to the flow with the shock present. This is the main reason a reference image was not used for Laser Sheet processing.

The Laser Sheet Subtraction Processing, used exclusively in Laser Sheet Mode, takes the absolute value of two consecutive flow images subtracted pixel by pixel.

The Reference Standard Deviation Processing, Flow Standard Deviation Processing, and Laser Sheet Subtraction Processing all result in an image where the pixel values are an indicator of pixel variability. Assuming that high variability indicates the presence of a shock, this "variability image" is scanned line by line using a subarray in the shape of an "X" to determine if all the pixels in the "X" area are greater than a certain threshold. The threshold used was equal to 3 standard deviations from the mean pixel intensity of the whole "variability image". The "X" subarray used in the Reference Standard Deviation and Flow Standard Deviation Processing is 21 pixels in size made up of a 3 by 3 pixel center, with four 3-pixel arms extending from the corners, as in Figure 14(a). The Laser Sheet Subtraction Processing used a smaller "X," seen in Figure 14(b). The 9 by 9 pixel and 4 by 4 pixel shapes scale inside the wind tunnel to 0.08- by 0.08-cm and 0.035- by 0.035-cm, respectively. The "X" subarray shape was chosen to utilize a shape larger than one pixel that would pick up significant spatial variation in pixel amplitude. The shape was large enough to ignore the smaller spatial variations that might be erroneously interpreted as a shock, but small enough to pick up the variations caused by the shock.

Red and green colors were used in the "X" subarray analysis as an aid for visualizing the shock location estimate. When the scanning "X" subarray contains pixels all of whose intensity is greater than 3 standard deviations from the "variability image" mean pixel intensity, then the center of the "X" subarray of pixels is marked with a green line which extends along the entire image column. A group of green lines together is assumed to be a shock location in the processed image. A red line was used to mark the center of a group of green lines. This red line was used as the calculated shock center in the results section.

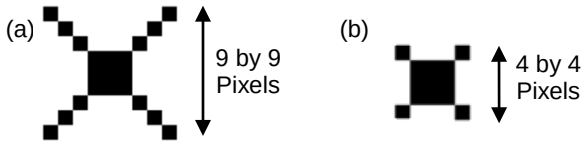

Figure 14.—"X" subarray used in the determination of the shock location for (a) Beam Scanning Mode and (b) Laser Sheet Mode.

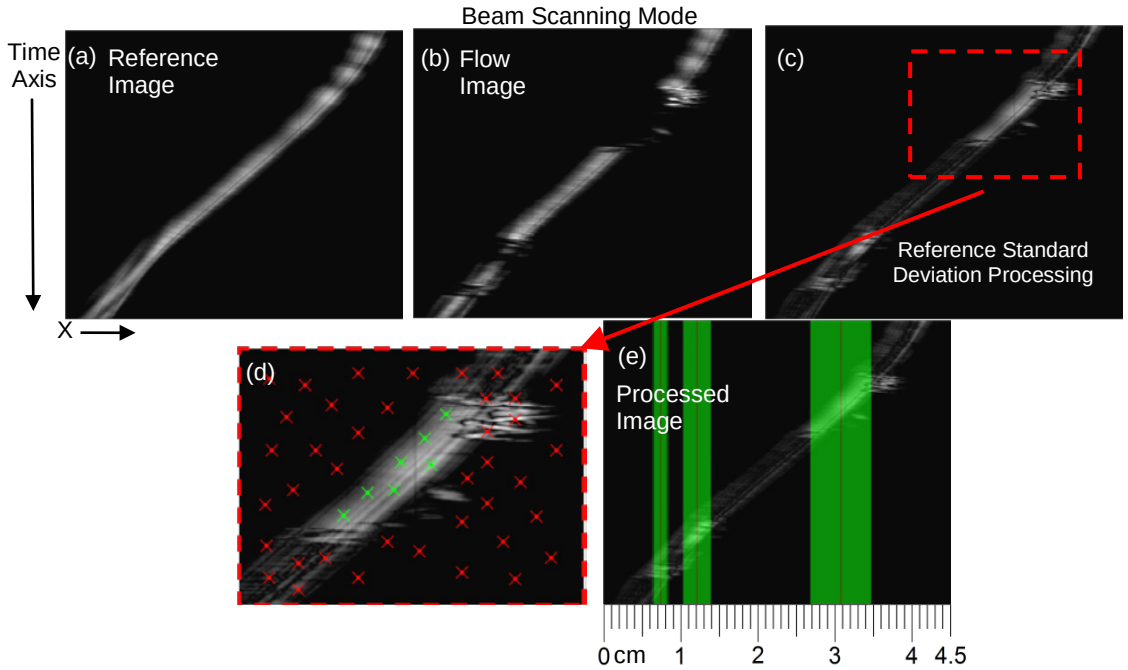

Figure 15.—Beam Scanning Mode image processing and shock location analysis for cases: (a) Reference image without flow present. (b) Image with the flow present and 9.65° ramp angle. (c) "Variability image" for Reference Standard Deviation Processing of the two previous images. (d) Zoomed in image of (c) demonstrating the "X" subarray analysis to determine the location of the shock, "X" subarray quantity and spacing not to scale. Green "X" subrarrays signify location of shock, red "X" subarrays do not. (e) Same as (c) but shows the shock location as determined by "X" subarray analysis shown in green with shock center locations approximately designated with a red line at 0.74, 1.21, and 3.08 cm, out of 4.5 cm scan width.

An example of the Reference Standard Deviation Processing is shown in Figure 15. The reference image is Figure 15(a). The flow image with ramp angle at 9.65° is shown in Figure 15(b). The pixel-by-pixel standard deviation using Figure 15(a) and 15(b) results in Figure 15(c), the "variability image," with the standard deviation scaled from dark to bright for display purposes, where bright indicates high variability. Figure 15(d) zooms into the location assumed to be the reflected shock location to show how the "X" subarrays are scanned across the image to determine the shock location. Although spacing between each "X" subarray is shown, actual analysis has a "X" subarray for every pixel, excluding the "X" subarrays that overlap the image edge. Figure 15(e) highlights the shock locations with green and paints the centers of the shock locations with a red line from left to right at 0.74, 1.21, and 3.08 cm, out of 4.5 cm scan width.

An example of the Flow Standard Deviation Processing is shown in Figure 16. Figure 16(a) is a "variability image" where each pixel represents the pixel-by-pixel standard deviation across 500 images and should be compared to Figure 15(c). The "X" subarray analysis of Figure 16(b) resulted in an image similar to Figure 15(e).

An example of the Laser Sheet Subtraction Processing is shown in Figure 17. The green area represents the shock location determined by "X" subarray analysis. Because the green area has separated areas, the average of the maximum and minimum, or the middle value, was calculated as the shock location for each image.

When comparing the reference and flow images in both the Beam Scanning and Laser Sheet Modes, the measurement noise generated in the wind tunnel shifted the flow image so that the reference image did not exactly map onto the scanned flow, even when a shock was not present. This explains the slight brightness in the standard deviation processing outside the two shock locations, such as in Figure 15(c), when it would be expected that the standard deviation would be 0 (a dark pixel).

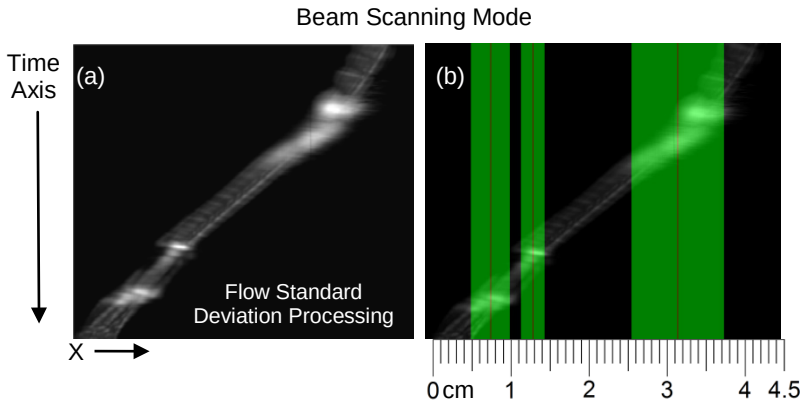

Figure 16.—(a) Beam Scanning Mode image processing and shock location analysis “variability image” for the Flow Standard Deviation Processing for 500 images. Flow present with 9.65° ramp angle. (b) “X” subarray analysis shown in green with shock center locations approximately designated with red line at 0.83, 1.36, and 3.19 cm, out of 4.5 cm scan width.

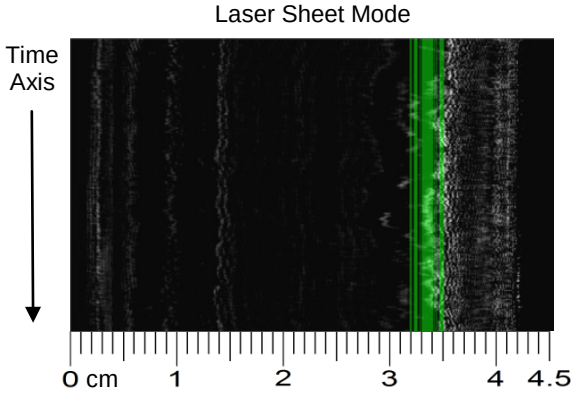

Figure 17.—“Variability image” for Laser Sheet Subtraction Processing and “X” subarray analysis for image with flow present and 9.65° ramp angle.

The data processed with the three ramp angles of 9.5°, 9.65°, and 9.8° are shown in the Table II to Table IV. The table values are the shock center locations as shown by the red line. Table II and Table III include results from the Beam Scanning Mode analysis at 126 Hz. In Table II the shock center location is estimated by averaging across multiple images using the Reference Standard Deviation Processing and “X” subarray analysis. In Table III the shock center location is estimated by Flow Standard Deviation Processing and “X” subarray analysis. In Table IV, shock center location is determined by Laser Sheet Subtraction Processing and “X” subarray analysis. Locations in all tables are given in centimeters out of a 4.5 cm scan width.

TABLE II.—ESTIMATED SHOCK LOCATIONS (cm) FOR DIFFERING RAMP ANGLES DETERMINED BY BEAM SCANNING MODE
[The location values are determined by averaging the results from Reference Standard Deviation Processing and Crosshair Analysis from several relatively stable flow images as determined by the experimenter at the designated ramp angle.]

Average Reference Standard Deviation Processing Results			
Ramp angle	9.5°	9.65°	9.8°
Incident shock a	0.78	0.75	0.69
Incident shock b	1.24	1.22	1.21
Reflected shock	3.51	3.18	2.74

TABLE III.—ESTIMATED SHOCK LOCATIONS (cm) FOR DIFFERING RAMP ANGLES DETERMINED BY BEAM SCANNING MODE
[The location values are determined by averaging the results from Flow Standard Deviation Processing for 500 images and Crosshair Analysis.]

Average Flow Standard Deviation Processing Results			
Ramp angle	9.5°	9.65°	9.8°
Incident shock a	0.84	0.83	0.78
Incident shock b	1.38	1.36	1.36
Reflected shock	3.52	3.19	2.79

TABLE IV.—ESTIMATED SHOCK LOCATIONS (cm) FOR DIFFERING RAMP ANGLES DETERMINED BY LASER SHEET MODE
[The location values are determined by averaging the results from Laser Sheet Subtraction Processing and Crosshair Analysis from several relatively stable flow images as determined by the experimenter at the designated ramp angle.]

Average Laser Sheet Subtraction Results			
Ramp angle	9.5°	9.65°	9.8°
Reflected shock	3.35	3.21	2.88

The results of the Reference Standard Deviation and Flow Standard Deviation Processing were in general agreement, as seen in Table II and Table III, but they had subtle differences. Due to the large number of images in the Flow Standard Deviation calculation, the resulting shock locations appear wider or more blurred in the variability image than they do in the reference standard deviation method. This is because the 500 images represent data across a greater time frame than the instantaneous reference standard deviation. As one might expect, the Flow Standard Deviation Processing resulted in a more consistent shock location, although such an analysis of a large number of images requires more computing power than the simple two image Reference Standard Deviation processing.
The results of the Laser Sheet Mode image processing shown in Table IV also correlated with results in Table II and Table III for the reflected shock only. Although the incident shock was observable during Laser Sheet Mode testing, the Laser Sheet Subtraction Processing and “X” subarray analysis could not detect the shock location because of the low signal to noise ratio at that particular shock location. A more consistently illuminated laser sheet and/or having a stronger shock would correct for this issue.

Conclusions

While a one-dimensional scanning approach to shock sensing has been shown to have the capability to detect the presence of a shock, there are some issues that must be addressed if the technique is to be useful as a stand-alone real-time shock measurement system.

One such issue is the difficulty in conclusively determining shock location. Comparing the results to Schlieren, two laser visualization techniques were investigated: Beam Scanning Mode, and Laser Sheet Mode. The Beam Scanning Mode demonstrated a laser beam shape transformation as the laser beam was passed through the shock. The Laser Sheet Mode demonstrated a high speed method capable of continuously scanning the flow. Results from these two techniques correlated well with the Schlieren results as well as with expected shock structure. Without the two-dimensional Schlieren images, it would be difficult to conclusively determine the shock location because of the one-dimensional nature of the approach. Another issue is noise. Noise and shocks have similar effects on the laser profile, so distinguishing between the two is often difficult. To fully explore the potential for the Beam Scanning Mode to determine shock properties such as strength and thickness, the technique must be able to see beam spreading, formation of tails and secondary fringes. In order to do so, the line camera must be oriented perpendicular to the projected shock line as seen, for example, in a Schlieren image. In this work the image line was fixed parallel to the flow direction and could not be adjusted perpendicular to the

projected shock line. Even if these issues were adequately addressed other issues such as complexity of the three-dimensional flow, and limitations on the angle and speed of the scanning hardware make determination of shock strength and thickness extremely unlikely. Image processing software was developed and succeeded in estimating the location of the shock, however, further development is necessary to meet fast real time processing requirements for in-flight instrumentation. Once these issues are resolved, the low weight and small size of components involved could lead to useful airborne applications for shock sensing inside ducts or tunnels where no optical access for Schlieren is possible.

References

1. Wilcox, F. A. and Perchonok, E., "Aerodynamic Control of Hypersonic Inlets for Optimum Performance," NACA Research Memorandum, NACA RM E55L1, 1956.
2. Albertson, C. W. and Venkan, V. S., "Shock Interaction Control for Scramjet Cowl Leading Edges," AIAA 2005-3289.
3. Cattafesta, L. N. III and Settles, G. S., "Experiments on Shock/Vortex Interaction," AIAA-92-0315.
4. Wright, M. J., Sinha, K., Olejniczak, J., and Candler, G. V., "Numerical and Experimental Investigation of Double-Cone Shock Interactions," AIAA Journal, Vol. 38, No. 12, pp. 2268-2276 (2000).
5. Adelgren, R. G., Yan, H., Elliott, G. S., Knight, D. D., Beutner, T. J., Zheltovodov, A. A., Ivanov, M., and Khotyanovsky, D., "Localized Flow Control by Laser Energy Deposition Applied to Edney IV Shock Impingement and Intersecting Shocks," Paper AIAA 2003-31.
6. Hewett, M. D., "High-Speed Civil Transport Issues and Technology Program," NASA CR-186020, 1992.
7. Ray, J. K, Carlin C. M., and Lambregts, A. A., "High-Speed Civil Transport Flight- Propulsion-Control Technological Issues," NASA CR-186015, 1992.
8. Sajben, M, Donovan, J. F., and Morris, M. J., "Flight Prototype Normal Shock Sensor," NASA CR-18520, 1990.
9. Iverson, D. G. Jr. and Daiber, T. D., "Flight Prototype Normal Shock Position Sensor," NASA CR-185204, 1989.
10. *Flow Visualization VII*, Proceedings of the Seventh International Symposium on Flow Visualization, September 11-14, 1995, Seattle, Washington, Ed. J. P. Crowder, Begell House, New York, 1995.
11. Shapiro, A. H., *The Dynamics and Thermodynamics of Compressible Fluid Flo*w, Volume I, The Ronald Press Company, New York, 1953, Chaps. 3.7.
12. Merzkirch, W., *Flow Visualization*, 2nd ed., Academic Press, New York, 1987.
13. Verna, S. B. and Koppenwallner, G., "Detection of Shock Motion Using Laser Schlieren System in a Hypersonic SWBLI Flowfield," AIAA 2001-1756.
14. Panda, J. and Adamovsky, G., "Laser Light Scattering by Shock Waves," American Institute of Phys., Vol. 7, No. 9, September 1995, pp. 2271-2279.
15. Adamovsky, G. and Johnson, D. K., "Optical Techniques for Shock Visualization and Detection," in *Optical Techniques in Fluid, Thermal, and Combustion Flows*, edited by S. S. Cha and J. D. Trolinger, SPIE Proceedings, Vol. 2546, 1995, pp. 348-357.
16. Adamovsky, G., "Scanning Mode Shock Position Sensor Invented and Demonstrated," in *Research & Technology 1998*, NASA/TM—1999-208815, 1999, p. 58.
17. Tokars, R., Adamovsky G., and Floyd B., "One-Dimensional Scanning Approach to Shock Sensing," Paper AIAA-2009-1454.
18. Balanis, C. A., *Advanced Engineering Electromagnetics*, John Wiley & Sons, New York, 1989, Chaps. 4 and 5.
19. Gaskill, J. D., *Linear Systems, Fourier Transforms, and Optics*, John Willey & Sons, New York, 1978, Chap. 10.
20. Keller, J. B., "Geometrical Theory of Diffraction," J. Opt. Soc. Am. Vol. 52, No. 2, pp. 116-130 (1962).

21. Chen, Y. M., “Diffraction by a Smooth Transparent Object,” J. Math. Physics 5, No. 6, pp. 820-832 (1964).
22. Ohtsuka, Y. and Cheah, Y. M., “Fresnel diffraction by a semitransparent straight edge object with acoustically coherence-controllable illumination,” Appl. Opt. Vol. 23, No. 2, pp. 300-306 (1984).
23. Nussenzveig, H. M., “High-Frequency Scattering by a Transparent Sphere. I. Direct Reflection and Transmission,” J. Math. Phys. Vol. 10, No.1, pp. 82-120 (1969).
24. Ganci, S., “Fraunhofer diffraction by a thin wire and Babinet’s principle,” *Am. J. Phys*., Vol. 73, No. 1, January 2005, pp. 83, 84.
25. Kozaki, S., “Scattering of a Gaussian beam by a homogeneous dielectric cylinder,” J. Appl. Phys. Vol. 53, No. 11, pp. 7195- 7200 (1982).
26. Adamovsky, G. and Ida, N., “Laser Beam Propagation Through Inhomogeneous Media,” in *Optical Technology in Fluid, Thermal, and Combustion flows III*, edited by S. S. Cha, J. D. Trolinger, and M. Kawahashi, SPIE Proceedings, Vol. 3172, 1997, pp. 530-539.
27. van Splunter, J. M., and van den Berg, P. M., “Spectral theory of diffraction of electromagnetic waves by a strip in the plane interface of semi-infinite media,” Can. J. Phys. Vol. 57, pp. 1148-1156 (1979).
28. Sanchez-Brea, L. M. and Salgado-Remacha, F. J.,” Three-dimensional diffraction of a thin metallic cylinder illuminated in conical incidence: application to diameter estimation,” Appl. Opt. Vol. 47, No. 26, pp. 4804-4811 (2008).
29. Khodier, S. A., “Measurement of wire diameter by optical diffraction,” Optics & Laser Technology Vol. 36, pp. 63-67 (2004).
30. Cowan, R. G. and Hornig, D. F., “The Experimental Determination of the Thickness of a Shock Front in a Gas,” J. Chem. Phys., Vol. 18, No. 8, 1950, pp. 1008-1018.
31. Greene, E. F., Cowan, R. G., and Hornig ,D. F., “The Thickness of Shock Fronts in Argon and Nitrogen and Rotational Heat Capacity Lags,” J. Chem. Phys., Vol. 19, No 4, 1951, pp. 427-434.
32. Porca, R. R., and Prenel, J.-P., “Visualization by means of coherent light sheets: application to different flows,” Optics and Laser Technology, October 1982.
33. Siegman, A. E., *Lasers*, University Science Books, Mill Valley, CA, 1986, Chap. 17.
34. *Pixis System Manual*, Princeton Instruments, User Manual 4411-0106 Version 1.D, January 18, 2006.
35. *Spyder 2 Camera User’s Manual*, DALSA, User Manual 03-32-10091-04, Version 04, 2005.

REPORT DOCUMENTATION PAGE	Form Approved OMB No. 0704-0188

1. REPORT DATE *(DD-MM-YYYY)*	2. REPORT TYPE	3. DATES COVERED *(From - To)*
01-03-2012	Technical Memorandum	

4. TITLE AND SUBTITLE
Wind Tunnel Testing of a One-Dimensional Laser Beam Scanning and Laser Sheet Approach to Shock Sensing

5a. CONTRACT NUMBER

5b. GRANT NUMBER

5c. PROGRAM ELEMENT NUMBER

6. AUTHOR(S)
Tokars, Roger; Adamovsky, Grigory; Anderson, Robert; Hirt, Stefanie; Huang, John; Floyd, Bertram

5d. PROJECT NUMBER

5e. TASK NUMBER

5f. WORK UNIT NUMBER
WBS 599489.02.07.03.01.05

7. PERFORMING ORGANIZATION NAME(S) AND ADDRESS(ES)
National Aeronautics and Space Administration
John H. Glenn Research Center at Lewis Field
Cleveland, Ohio 44135-3191

8. PERFORMING ORGANIZATION REPORT NUMBER
E-18170

9. SPONSORING/MONITORING AGENCY NAME(S) AND ADDRESS(ES)
National Aeronautics and Space Administration
Washington, DC 20546-0001

10. SPONSORING/MONITOR'S ACRONYM(S)
NASA

11. SPONSORING/MONITORING REPORT NUMBER
NASA/TM-2012-217439

12. DISTRIBUTION/AVAILABILITY STATEMENT
Unclassified-Unlimited
Subject Categories: 06, 34, 35, 61, and 36
Available electronically at http://www.sti.nasa.gov
This publication is available from the NASA Center for AeroSpace Information, 443-757-5802

13. SUPPLEMENTARY NOTES

14. ABSTRACT
A 15- by 15-cm supersonic wind tunnel application of a one-dimensional laser beam scanning approach to shock sensing is presented. The measurement system design allowed easy switching between a focused beam and a laser sheet mode for comparison purposes. The scanning results were compared to images from the tunnel Schlieren imaging system. The tests revealed detectable changes in the laser beam in the presence of shocks. The results lend support to the use of the one-dimensional scanning beam approach for detecting and locating shocks in a flow, but some issues must be addressed in regards to noise and other limitations of the system.

15. SUBJECT TERMS
Optics; Shadowgraph photography; Schlieren photography; Hypersonic wind tunnels

16. SECURITY CLASSIFICATION OF:			17. LIMITATION OF ABSTRACT	18. NUMBER OF PAGES	19a. NAME OF RESPONSIBLE PERSON
a. REPORT	b. ABSTRACT	c. THIS PAGE			STI Help Desk (email:help@sti.nasa.gov)
U	U	U	UU	26	19b. TELEPHONE NUMBER *(include area code)* 443-757-5802